CHAPTER 3

HOT CORROSION BEHAVIOR OF SUPERALLOY IN718 AT 600ºC

3.1 INTRODUCTION

Marine gas turbines operate in the environments where ingestion of solid particles of NaCl with air is unavoidable and leads to their corrosion at elevated temperature. High strength and corrosion resistance material is needed for power generation and aero engine applications. Ni-Fe based superalloy IN718 is mostly used in turbine and compressor components of advanced power plants and aero engines **[Sundararaman et al. (1988)]**. Although Ni-base superalloys possess adequate strength at the operating temperatures of turbines, they suffer from hot corrosion due to deposition of salts in the operating environments **[Collier et al. (1988), Lai (2007)]**. It is well known that for hot corrosion, salt must be in molten state to accelerate the oxidation and sulfidation of superalloys at elevated temperatures. Hot corrosion is of two types; the high temperature hot corrosion (HTHC) occurring above 750ºC to 950ºC and low temperature hot corrosion (LTHC) in the temperature range of 550ºC to 750ºC. In the HTHC, Na_2SO_4 is in molten state whereas in the LTHC the eutectic Na_2SO_4-MSO_4 (M = Ni, Co and Fe) undergoes to molten state **[Eliaz et al. 2002, Mahobia et al. (2013), Mannava et al. (2016)]**.

Several means are being used to modify the surface and develop nanostructure. Ultrasonic shot peening is a relatively new process of generating surface nanostructure.

Mechanical properties of metallic materials are significantly improved by surface nanostructuring without changing their chemical compositions **[Kumar et al. (2014)]**. Effect of surface grain refinement by shot peening was studied on oxidation behavior of the Inconel 800 alloy and improvement in oxidation resistance was observed. Similar enhancement in oxidation resistance from surface nanostructuring has also been observed in zirconium **[Zhang et al. (2007)].** The effect of surface nanostructuring from ultrasonic shot peening was studied on hot corrosion behavior of Ti–6Al–4V, at 400, 500 and 600 °C and the hot corrosion resistance was found to improve due to ultrasonic shot peening **[Kumar et al. (2016)]**. However, there is no report on the effect of ultrasonic shot peening on hot corrosion behavior of the superalloy IN718.

Surface of compressor and turbine components undergo repetitive erosion and corrosion due to impingement of high velocity NaCl particles which makes the surface rough in service. Therefore, the present investigation was undertaken to study the effect of surface roughness on hot corrosion behavior of the alloy IN718 coated with single salt 1S (100 wt% NaCl), two salt mixture 2SM (60 wt% Na_2SO_4+ 40wt % V_2O_5) and three salt mixture 3SM (75 wt% Na_2SO_4 + 15 wt% NaCl + 10 wt% V_2O_5) in air at 600ºC for 100 h. In addition, the effect of ultrasonic shot peening is studied on hot corrosion resistance of this alloy in the salt mixture 2SM at 700ºC.

3.2 RESULTS

3.2.1 MICROSTRUCTURAL CHARACTERIZATION

The microstructure of the superalloy IN718 was characterized by optical and scanning electron microscopy (SEM) before and after the hot corrosion. For optical microscopy and SEM, samples were etched with Kalling's reagent No. 2 containing 5g $CuCl_2$, 100 ml HCl, and 100 ml ethanol. Also, samples of different surface roughness were examined under

SEM. Optical micrograph of the peak aged specimen showed equiaxed grains with mean intercept length of ≈ 16 μm (Fig. 3.1 (a)). Plate type δ phase particles were revealed by SEM and TEM micrograph, distributed mainly at grain boundaries (Fig. 3.1 (b & c)).

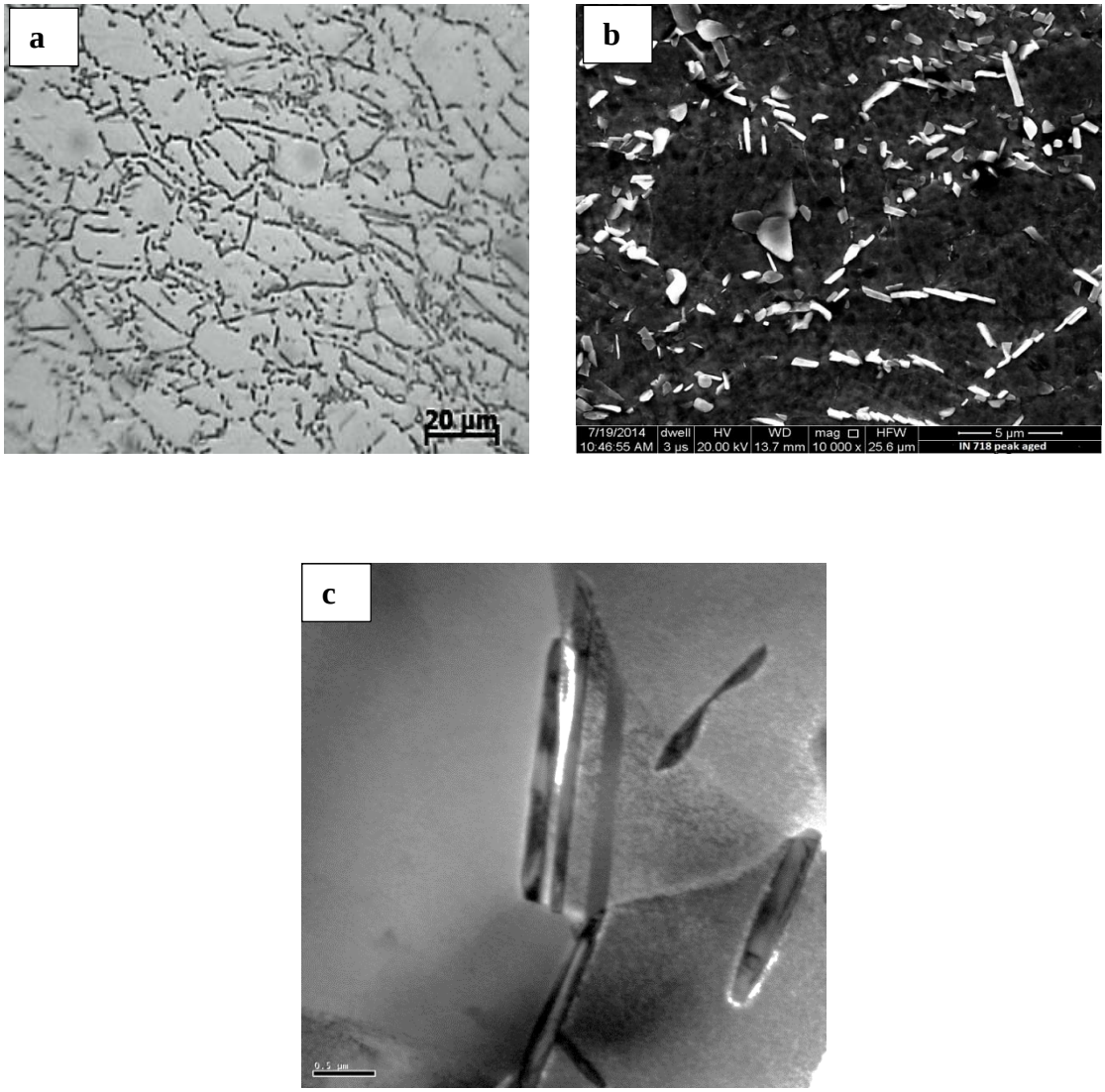

Fig. 3. 1: Microstructure of the peak aged superalloy IN718 (a) optical micrograpgh, (b) SEM micrograph and (c) TEM micrograph.

Grain refinement in the USP treated condition is substantiated from the discontinuous selected area diffraction (SAD) ring patterns (Fig. 3.2). The process of grain refinement in the surface layer by USP involves severe plastic deformation from continual multidirectional mechanical impacts of hardened steel balls at very high speed, on the surface of the specimen. Clustering of diffraction spots in some rings of diffraction pattern suggests a common crystallographic direction of many nano size grains and thus tendency for preferred orientation. The average size of the USP treated surface was found to be 71-92 nm up to the depth of ~ 58 μm from the USP treated surface.

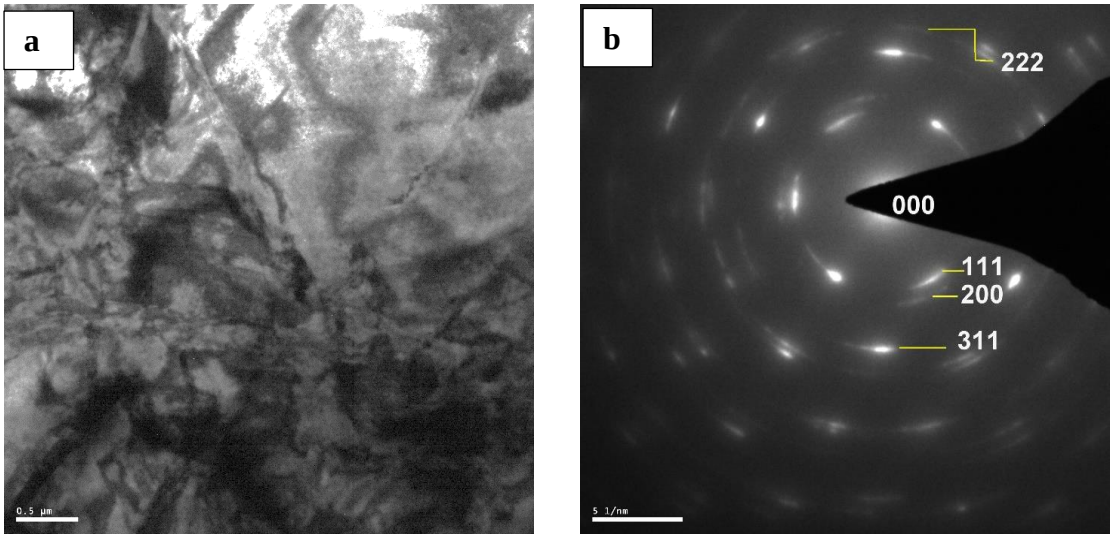

Fig. 3. 2: Bright field TEM micrograph and the corresponding SAD pattern of the superalloy IN718 subjected to ultrasonic shot peening for 5 min.

3.2.2 DISLOCATION DENSITY AND MICROHARDNESS

Dislocation density (ρ) of the samples ground with 1000 (R_{a1}), 800 (R_{a2}), 600 (R_{a3}) and 400 (R_{a4}) grit SiC emery papers was calculated by XRD and using the relationship given below **[Dini et al. (2010)]**:

$$\rho = \frac{3\sqrt{2\pi}}{Db}\left(\varepsilon^2\right)^{1/2} \tag{3.1}$$

where D is average crystallite size (Scherrer and Wilson equation **[Lanford et al. (1978)]**, $D = \frac{0.9\lambda}{B\cos\theta}$), ε is microstrain (Williamson Hall equation **[Williamson et al. (1953)]**, $B\cos\theta = \frac{0.9\lambda}{D} + 4\varepsilon\sin\theta$, where λ is X-ray wavelength, θ is Bragg angle and B is line broadening) , b is Burgers vector (b = a/$\sqrt{2}$ for FCC structure) and a is lattice parameter. The dislocation density corresponding to average roughness of R_{a1}, R_{a2}, R_{a3}, and R_{a4} was estimated to be 1.9 X 10^9 m^{-2} (ρ_1), 2.48 X 10^9 m^{-2} (ρ_2), 2.66 X 10^9 m^{-2} (ρ_3), and 4.68 X 10^9 m^{-2} (ρ_4) respectively, using XRD. It is evident from Fig. 3.3 (a) that dislocation density increases with surface roughness.

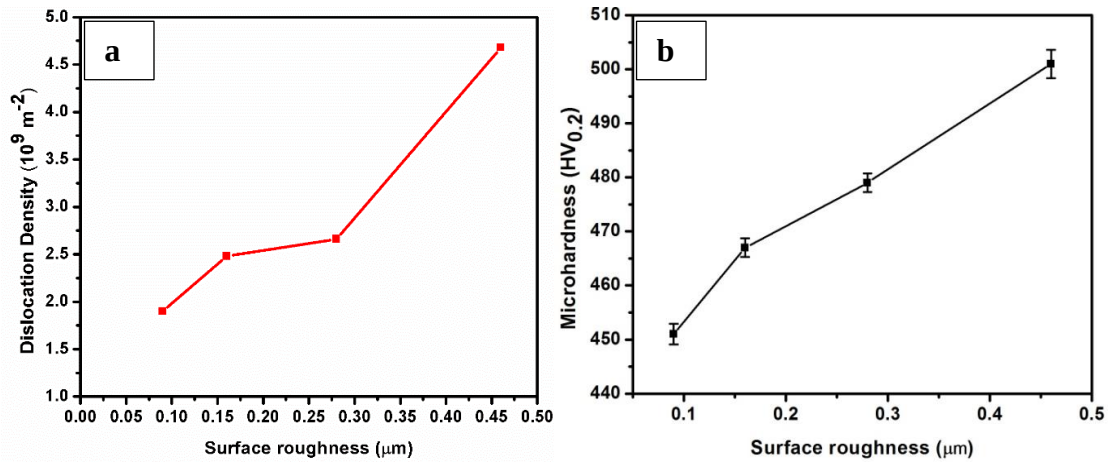

Fig. 3. 3: Effect of surface roughness on: (a) dislocation density and (b) microhardness.

Fig. 3.3 (b) shows variation of microhardness of the samples, ground with 1000 (R_{a1}), 800 (R_{a2}), 600 (R_{a3}) and 400 (R_{a4}) grit emery papers with R_a: 0.09 µm, 0.16 µm, 0.28 µm and 0.46 µm, respectively. Microhardness of the samples with surface roughness R_{a1}, R_{a2}, R_{a3}, and R_{a4} was 451±1.9 HV, 466±1.7 HV, 479±1.7 HV and 501±2.7 HV

respectively. Thus, microhardness of the samples gradually increased with increase in the surface roughness (Fig. 3.3 b).

3.2.3 GRAIN SIZE MEASUREMENT OF THE ULTRASONIC SHOT PEENED SAMPLES

The grain refinement and microstructural phases were characterized using XRD analysis. Peaks of γ, γ' and γ'' are shown in Fig. 3.4 for the un-shot peened and 5 min USP treated samples. The matrix is γ whereas γ' and γ'' are precipitate phases of $Ni_3(Al, Ti)$ and Ni_3Nb with FCC and BCT crystal structure, respectively. No phase change was observed due to ultrasonic shot peening, however, there was peak broadening in the 5 min USP treated sample in respect of the untreated one. The average grain size of the USP treated samples was calculated using the Scherrer and Wilson equation **[Langford et al. (1978)].**

$$D = \frac{0.9\lambda}{B\cos\theta} \tag{3.2}$$

where λ is X-ray wavelength, θ is Bragg angle and B is line broadening. The average grain size of the sample USP treated for 5 min was found to be about 82 nm.

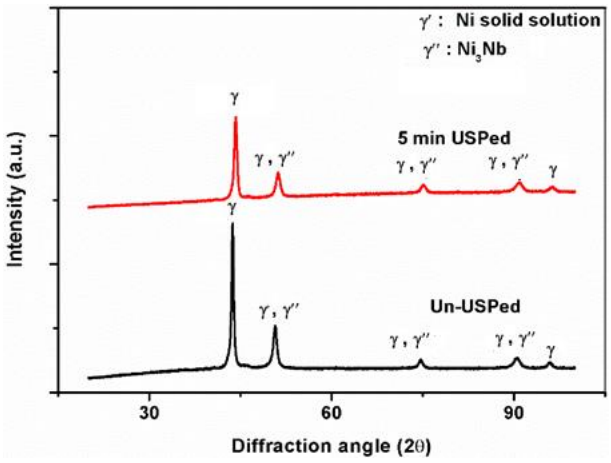

Fig. 3. 4: X-ray diffraction of un-shot peened and ultrasonic shot peened superalloy IN718.

3.2.4 VISUAL OBSERVATIONS

The hot corroded samples with different surface finish were visually examined after every heating cycle. The features of the corrosion scale were recorded using a digital camera which are shown in Fig. 3.5.

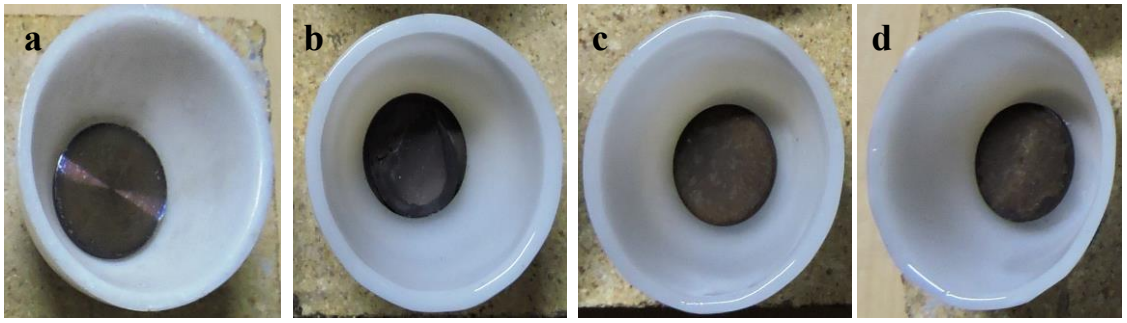

For 0.5 h

(a) Uncoated (b) 1S coated (c) 2SM coated (d) 3SM coated

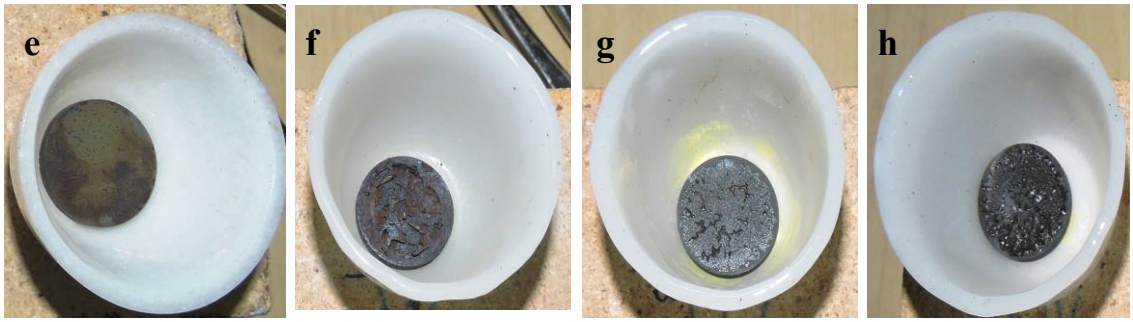

For 100 h

(e) Uncoated (f) 1S coated (g) 2SM coated (h) 3SM coated

Fig. 3. 5: Digital photographs of the #400 grit ground samples oxidized/hot corroded at 600ºC for 0.5 h (a-d) and 100 h (e-h).

Table 3.1 presents the details of visual observations of the samples oxidized and corroded at 600°C for 100 h. There was no effect of the surface roughness on colour and scale characteristics of the different salt coated samples.

Table 3.1: Visual observation of the samples oxidized/hot corroded at 600ºC up to 100 h

Salt Coating	Colour	Scale characteristics
Uncoated	Dark gray	No scale formation, adherent oxide layer formed.
1S	Dark reddish brown	Heavy scaling, formation of fragile scale and spalling of the scale.
2SM	Dark gray	Adherent coating without spalling.
3SM	Gray with yellow visible spots on the surface	Very less scaling with less porosity in oxide layer.

3.2.5 CORROSION KINETICS

The plots of weight gain per unit area vs time (Figs. 3.6 to 3.8) clearly show the influence of the coatings of one salt and salt mixtures on hot corrosion behavior of the superalloy IN718. The effect of surface roughness can be seen in all the salt coated samples. Rough surfaces showed more corrosion rate as compared to the smooth ones. Weight gain was not observed in the uncoated samples exposed at 600ºC, up to 100 h. However, weight gain was significant in the samples coated with 1S salt whereas there was less weight gain in the samples coated with 2SM and 3SM salt mixtures. The Cl^- ions are highly volatile as compared to sulphates and vandates. Oxychlorination reaction takes place in the case of 1S salt coated samples and it takes place also at lower temperature **[Mahobia et al. (2013), Mannava et al. (2016)]**. Therefore, the corrosion is mainly by the process of sulfidation in the case of 2SM coated samples where there is total absence of NaCl. On the other hand there is combined effect of oxychlorination and sulfidation in the 3SM coated samples where there is 15% NaCl in the coating. Thus, the slower rate of oxidation in the 2SM coated sample may be attributed to formation of an adherent and continuous protective oxide layer and absence of the chloride ions.

The plots of square of the weight gain per unit area vs time of exposure at 600ºC for the period up to 100 h, with different surface roughness are shown in Figs. 3.6-3.8. A close examination of these plots shows that the weight gain was higher during the initial 25 h in almost all the salt coated samples. The observed corrosion rate may be attributed to rapid formation of oxides in the beginning and penetration of the oxidizing ions through open pores of the oxide layer, however, the subsequent gain in weight became gradual. The salt/salt mixture coated samples show nearly parabolic behavior for the entire period of corrosion up to 100 h of exposure. Figs. 3.6 (a), 3.7 (a) and 3.8 (a) show the variation of weight gain per unit area vs time of exposure up to 100 h. The samples coated with 1S salt and the salt mixtures 2SM and 3SM show dual slope behavior. The plots of square of weight gain/area (mg^2/cm^4) versus time of exposure (h) (Figs. 3.6 (b), 3.7 (b)) and 3.8 (b)) were used to establish the rate law for the process of hot corrosion.

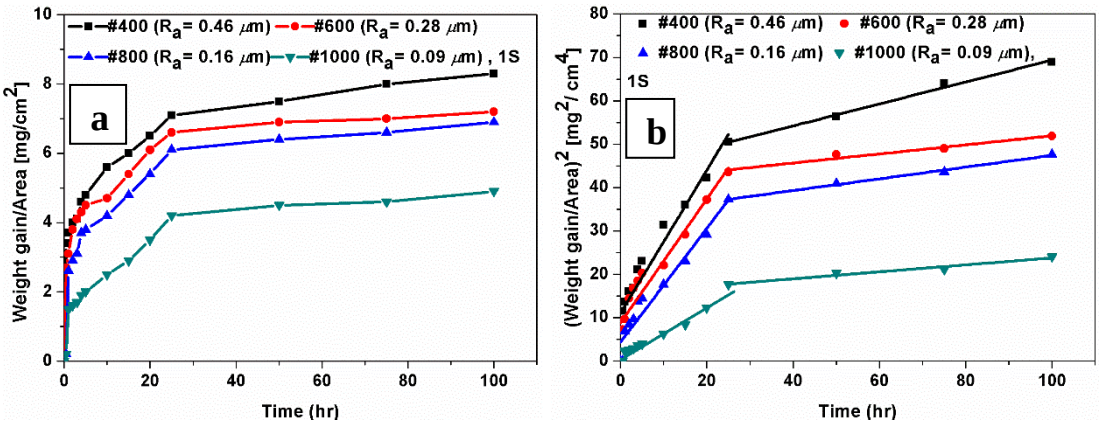

Fig. 3. 6: Effect of surface roughness on corrosion behavior of the specimens coated with 1S salt and exposed at 600ºC up to 100 h: (a) Weight gain per unit area vs time; (b) square of weight gain per unit area vs time.

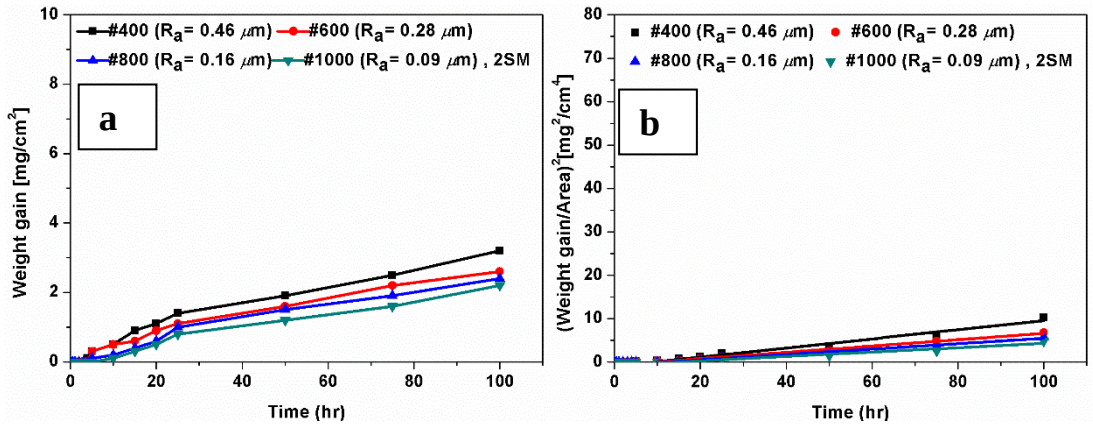

Fig. 3. 7: Effect of surface roughness on corrosion behavior of the specimens coated with 2SM salt mixture and exposed at 600ºC up to 100 h: (a) Weight gain per unit area vs time; (b) square of weight gain per unit area vs time.

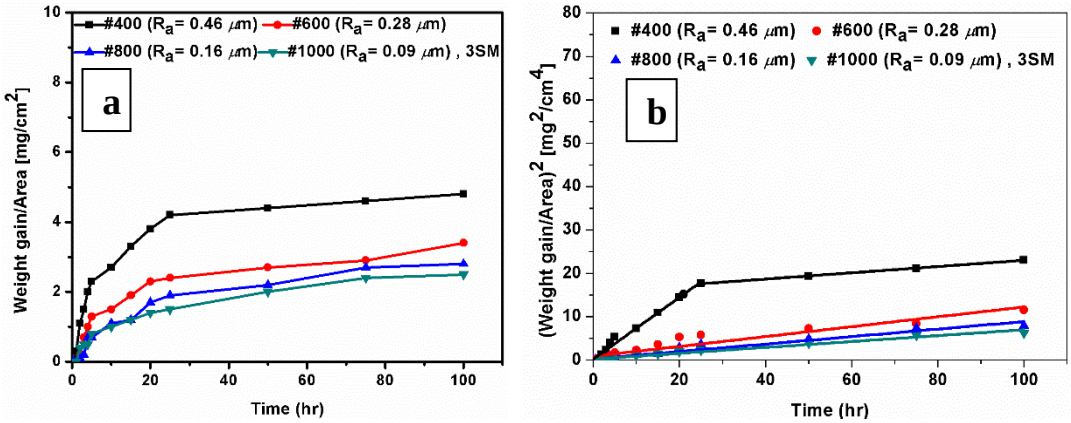

Fig. 3. 8: Effect of surface roughness on corrosion behavior of the specimens coated with 3SM salt mixture and exposed at 600ºC up to 100 h: (a) Weight gain per unit area vs time; (b) square of weight gain per unit area vs time.

Table 3.2: Parabolic rate constant (k_p) of the samples with different roughness, corroded at 600^0C up to 100 h.

Material Condition	**#400 (R_a = 0.46 µm)**		**#600 (R_a = 0.28 µm)**		**#800 (R_a = 0.16 µm)**		**#1000 (R_a = 0.09 µm)**	
	k_p	R^2	k_p	R^2	k_p	R^2	k_p	R^2
1S								
Up to 25 h	1.64	0.91	1.42	0.90	1.31	0.93	0.62	0.96
Up to 100 h	0.25	0.98	0.13	0.94	0.10	0.99	0.08	0.95
2SM								
Up to 25 h	0.10	0.97	0.07	0.99	0.06	0.98	0.05	0.97
Up to 100 h	0.10	0.97	0.07	0.99	0.06	0.98	0.05	0.97
3SM								
Up to 25 h	0.71	0.98	0.24	0.98	0.14	0.95	0.09	0.95
25 to 100 h	0.07	0.99	0.24	0.98	0.14	0.95	0.09	0.95

***k_p is in $mg^2 cm^{-4} h^{-1}$**

The parabolic rate constant k_p was calculated using the Pilling and Bedworth equation **[Pilling et al. (1923)]**: $(\Delta W/A)^2 = k_p * t + C$, where $\Delta W/A$ is weight gain per unit surface area (mg/cm^2), t is the time of exposure and C is a constant. Figs. 3.6 (b) show two linear segments with different slopes for the different surface roughness and suggest parabolic nature of corrosion at two different rates. Two segments are also seen in Fig. 3.8 b for the roughest surface (#400). Calculated values of the parabolic rate

constant are shown in Table 3.2. A higher value of k_p implies a faster rate of oxidation at a given temperature. The value of k_p was found to be maximum in the case of 1S coating from exposure at 600ºC. The plots of weight gain were best fitted by linear least square method and the calculated values of k_P are presented in the Table 3.2. It is obvious from Table 3.2 that the value of k_p is higher for the samples coated with 1S salt for all the surface roughness as compared with the samples coated with 3SM and2SM salt mixtures respectively. Further, k_p is higher for the most roughened surface of #400 grit in all the salt coated samples.

3.2.6 DEPTH OF PENETRATION OF CORRODANT

The hot corroded samples after 100 h of exposure were sectioned to study the depth of penetration and the mechanism of corrosion on different surface roughness. Figs. 3.9 - 3.11 clearly show that the depth of penetration of corrodants increased with increasing surface roughness. The depth of penetration in the samples ground with emery paper of 400 grit was found to be maximum in the all types of salt/salt mixture. In the 1000 grit ground samples the depth of attack was minimum in the all types of coatings.

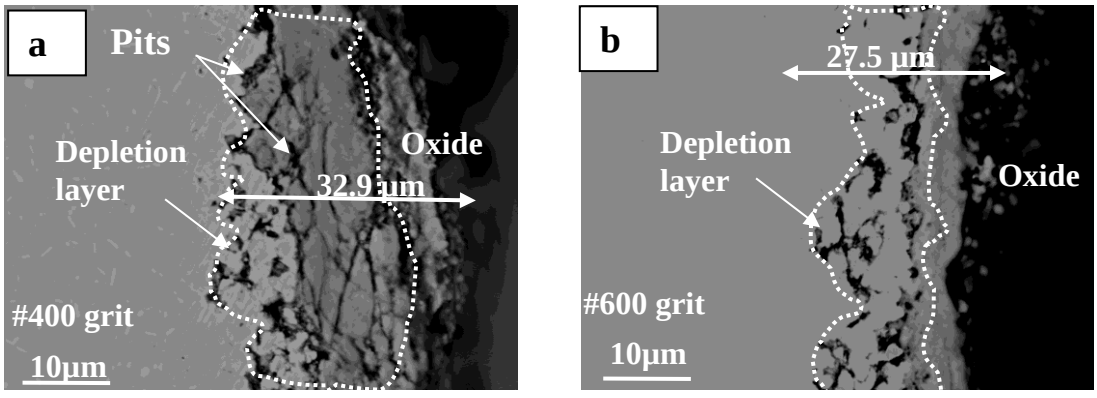

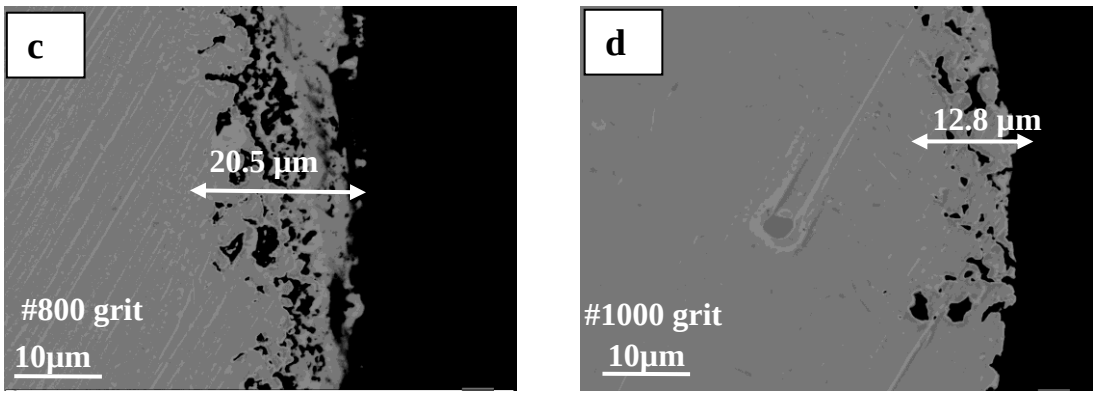

Fig. 3. 9: SEM micrographs showing the effect of different surface roughness on the depth of penetration of corrodants in the samples coated with 1S salt and exposed at 600ºC for 100 h: (a) #400, (b) #600, (c) #800 and (d) #1000

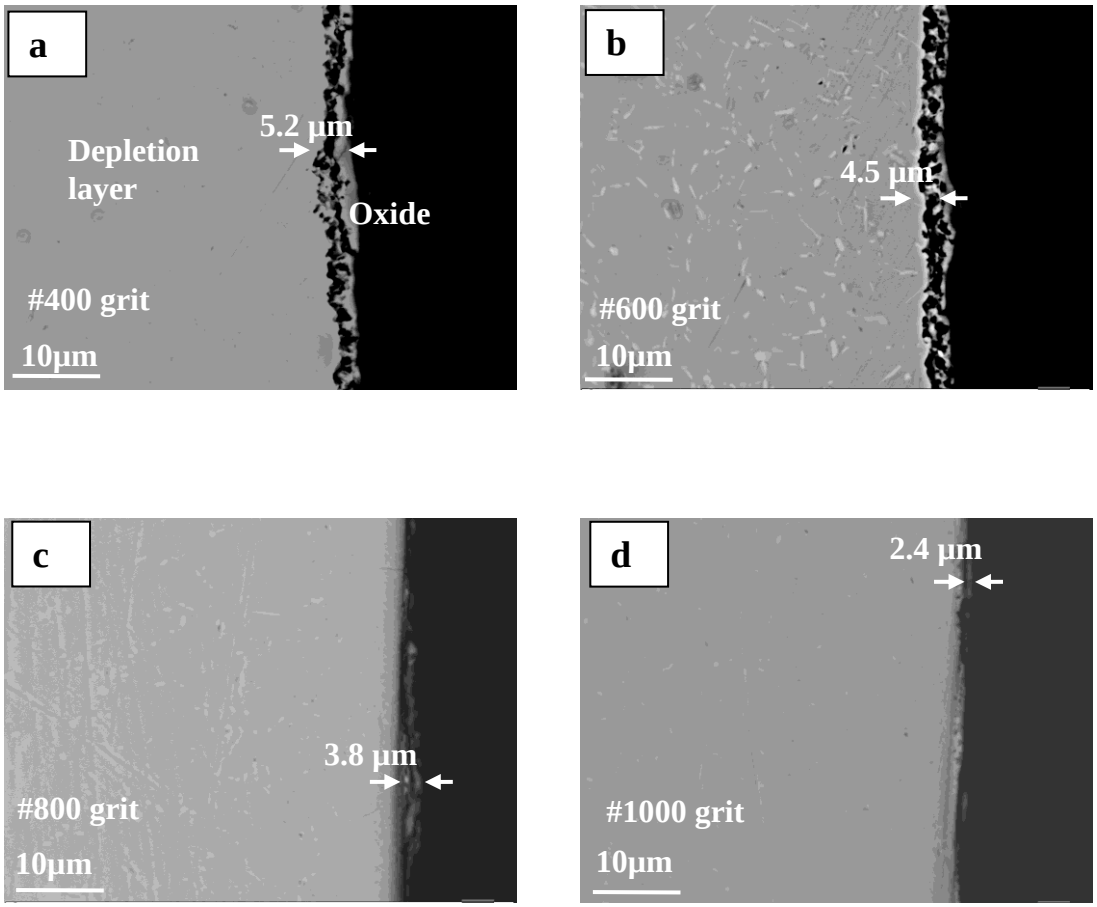

Fig. 3. 10: SEM micrographs showing the effect of surface roughness on the depth of penetration of corrodants in the samples coated with 2SM salt and exposed at 600ºC for 100 h: (a) #400, (b) #600, (c) #800 and (d) #1000

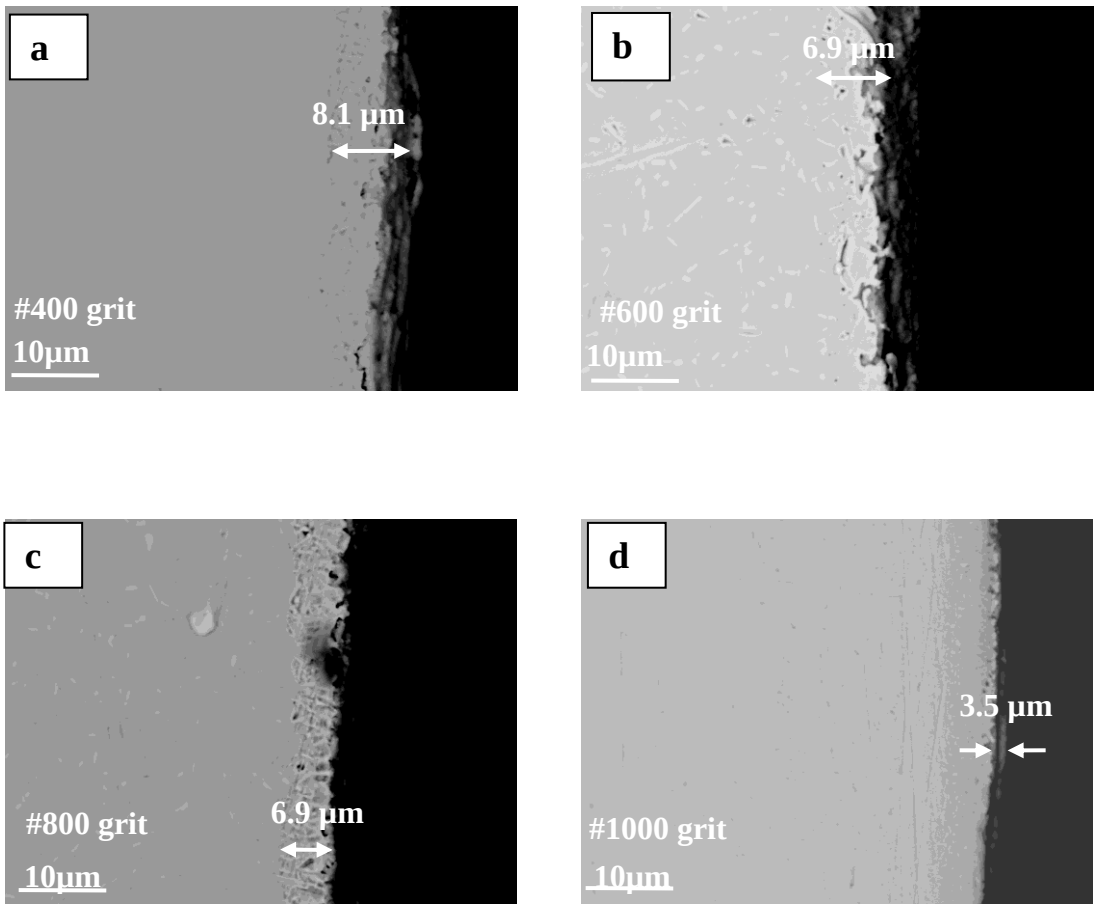

Fig. 3. 11: SEM micrographs showing the effect of surface roughness on the depth of penetration of corrodants in the samples coated with 3SM salt and exposed at 600ºC for 100 h: (a) #400, (b) #600, (c) #800 and (d) #1000.

BSE images of the NaCl (1S) coated samples, exposed up to 100 h at 600ºC clearly indicated formation of depletion layers. Pits were formed due to penetration of NaCl salt in the sample causing damage of the surface by oxychlorination reaction (Fig. 3.9). In case of the samples coated with the salt mixtures 2SM and 3SM, the depth of attack was smaller as compared to those of the 1S salt coated samples. The corrosion was mainly by the process of sulfidation (more effective above 700°C) in case of 2SM coated samples (Fig. 3.10) whereas in the 3SM coated sample (Fig. 3.11), there was combined effect of oxychlorination and sulfidation reactions. Therefore, the depth of attack was found to be less for the 2SM coated sample.

3.2.7 PHASES IN THE OXIDE FILMS

The nature of the phases formed during the salt induced corrosion can influence the rate of corrosion of the material. The XRD patterns of the uncoated and salt coated samples, following exposure of 100 h at 600ºC are shown in Figs. 3.12 (a, b, c & d). The main phases identified from the X-ray diffraction analysis of the uncoated sample were γ (Ni solid solution), Cr_2O_3, Ni_3Nb, $Ni_3(Al,Ti)$ and there was no sign of any new phase after its exposure at 600ºC for 100 h. However, in the case of salt coated samples several complex oxides formed and these are presented in Table 3.3. The nature of the oxide scale formed was found to be unaffected by the surface roughness.

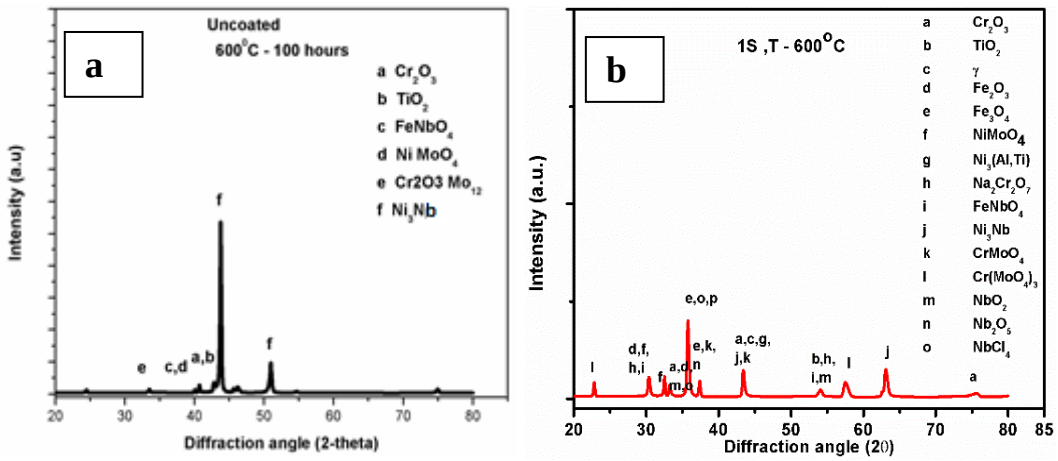

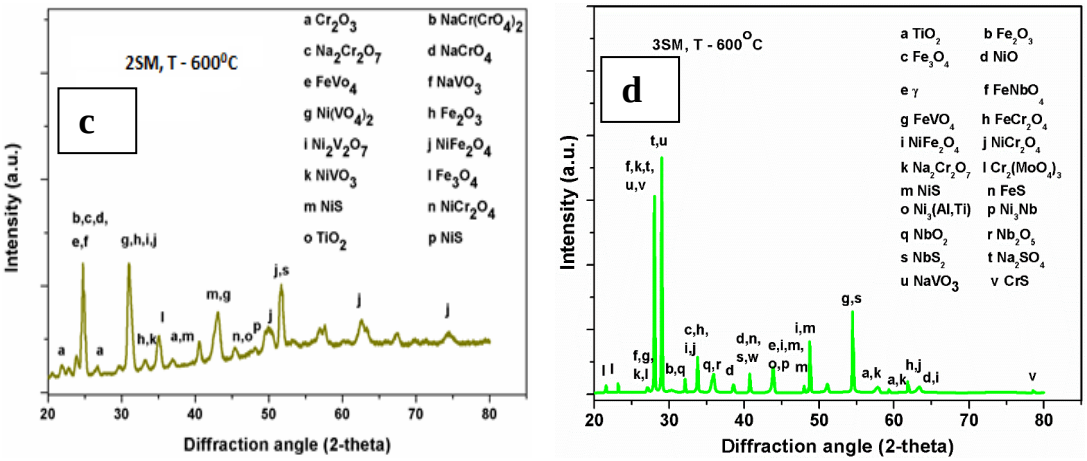

Fig. 3. 12: X-ray diffraction patterns of the uncoated sample and those coated with different salt/salt mixtures exposed at 600ºC, up to 100 h: (a) uncoated, (b) coated with 1S salt (100 wt% NaCl), (c) coated with salt mixture 2SM (60 wt% Na_2SO_4 + 40 wt% V_2O_5) and (d) coated with salt mixture 3SM (75 wt% Na_2SO_4 + 15 wt% NaCl + 10 wt% V_2O_5).

Table 3. 3: The phases formed on the samples corroded by 1S, 2SM and 3SM at 600ºC, up to 100 h of exposure

Type of coating	**Phases found after 100 h of exposure at 600^{0}C**
1S	Fe_2O_3, Fe_3O_4, Cr_2O_3, $FeCr_2O_4$, Ni_2CrO_4, $NiFe_2O_4$, NiO, $NiFe_2O_4$, Na_2CrO_4, $Na_2Cr_2O_7$
2SM	Cr_2O_3, Fe_3O_4, Ni_3Nb, $Ni(VO_3)_2$, $FeVO_4$, Fe_2VO4 Ni_3Al, Fe_2O_3, FeS, $Na_2Cr_2O_7$, CrS
3SM	Ni_3Al, $Ni(VO_3)_2$, Ni_2CrO_4, Ni_3Nb, $NaCrO_2$, $Na_2Cr_2O_7$, Fe_2O_3, Fe_3O_4, $Ni_2V_2O_7$, $FeCr_2O_4$, $NiCr_2O_4$, $NiFe_2O_4$, $FeVO_4$

3.2.8 SURFACE MORPHOLOGY AND COMPOSITION

Surface features of the hot corroded samples were examined under SEM to understand the characteristics of the scales (Figs. 3.13 to 3.15). The SEM micrographs revealed that the attack was non uniform. The 1S coated sample showed formation of globular oxides with heavy spallation whereas the 2SM coated sample revealed formation of flaky and cuboidal oxides. On the other hand non uniform oxides were seen on the sample coated with 3SM and there was less spallation of oxides. EDS analysis of the hot corroded samples revealed the presence of various elements associated with their respective oxides (Table 3.3). The high percentage of Fe and Ni confirmed the heavy scaling resulting from rapid growth of their oxides. The presence of chloride (Cl) supports the formation of $FeCl_3$ and $CrCl_3$ in addition to Cr_2O_3 and Fe_3O_4 in the case of NaCl coated sample exposed at 600ºC. The presence of sodium (Na) confirms the formation of Na_2CrO_4 along with Cr_2O_3 and Fe_3O_4. EDS analysis of the 2SM coated sample, exposed at 600°C, showed the presence of $NiFe_2O_4$ and $Ni(VO_3)_2$ in addition to Cr_2O_3 and Fe_3O_4. Here, the growth of Fe_3O_4 and NiO was less as compared with that of the 1S salt and 3SM salt mixture coated samples, therefore the scale was more adherent. In the case of the 3SM coated sample exposed at 600ºC, presence of vanadium led to formation of $Ni(VO_3)_2$ in addition to oxides of Fe, Cr and Ni. The surface morphology and compositions remained unaffected by the surface finish.

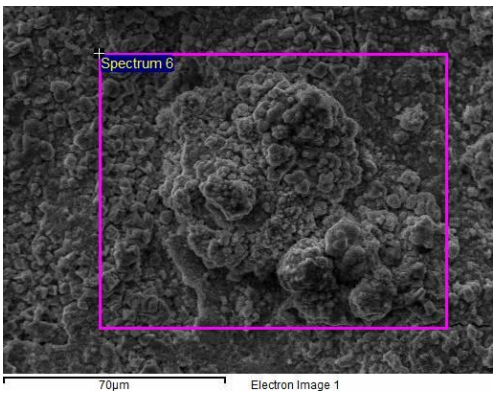

Element	Weight %
O	27.1
Ti	0.5
Cr	5.6
Fe	43.7
Ni	19.1
Nb	4.0

Fig. 3. 13: SEM micrograph showing morphology of the 1S salt coated sample exposed at 600ºC for 100 h. The EDS analysis shows concentration of the different elements.

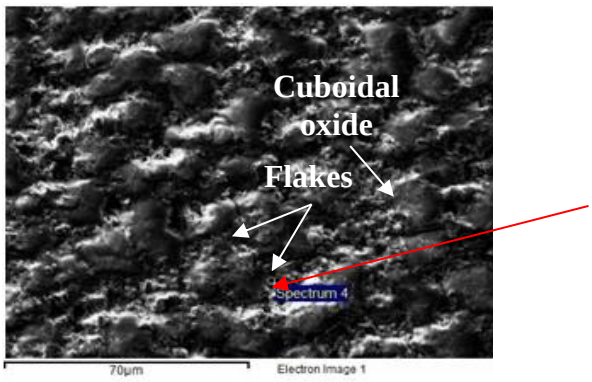

Element	Weight %
O	34.5
Ti	6.4
V	2
Cr	12.3
Fe	10.4
Ni	6.2
Nb	28.2

Fig. 3. 14: SEM micrograph showing morphology of the sample coated with salt mixture 2SM and exposed at 600ºC for 100 h. The EDS analysis shows concentration of the different elements.

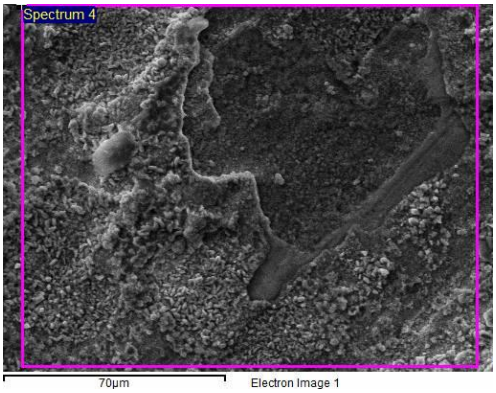

Element	Weight %
O	32.1
S	0.3
Cl	0.2
Ti	1.1
V	1.3
Cr	26.3
Fe	21.8
Ni	12.6
Nb	4.3

Fig. 3. 15: SEM micrograph showing morphology of the sample coated with salt mixture 3SM and exposed at 600ºC for 100 h. The EDS analysis shows concentration of the different elements.

3.2.9 ELECTRON PROBE MICRO ANALYSIS (EPMA) OF THE CROSS SECTIONS

In order to further examine the depth of the scales formed and the inward mode of transfer of corrodants, the cross sections of the hot corroded samples were examined. Wave length dispersive spectroscopy (WDS) was used for elemental mapping and EPMA was used for the elemental distribution (Figs. 3.16 to 3.21). The sample ground with #400 grit emery paper suffered maximum corrosive attack due to high surface roughness. It is important to mention that dense oxide scale formed and also there was spalling of the scale in case of the 1S coated sample (Figs. 3.16 and 3.17) in agreement with earlier investigation [16] whereas less dense oxides were formed in the 3SM and 2SM coated samples exposed at 600ºC up to 100 h . The elemental maps revealed variation in distribution of nickel, iron, chromium and oxygen in the hot corroded samples. It may be seen that the region of distribution of oxygen is more in the 1S coated sample than those in the 3SM and 2SM coated samples. The diffusion of nickel, iron and chromium from the base material towards the surface of the substrate resulted in formation of NiO, Fe_2O_3, Fe_3O_4, Cr_2O_3 oxides.

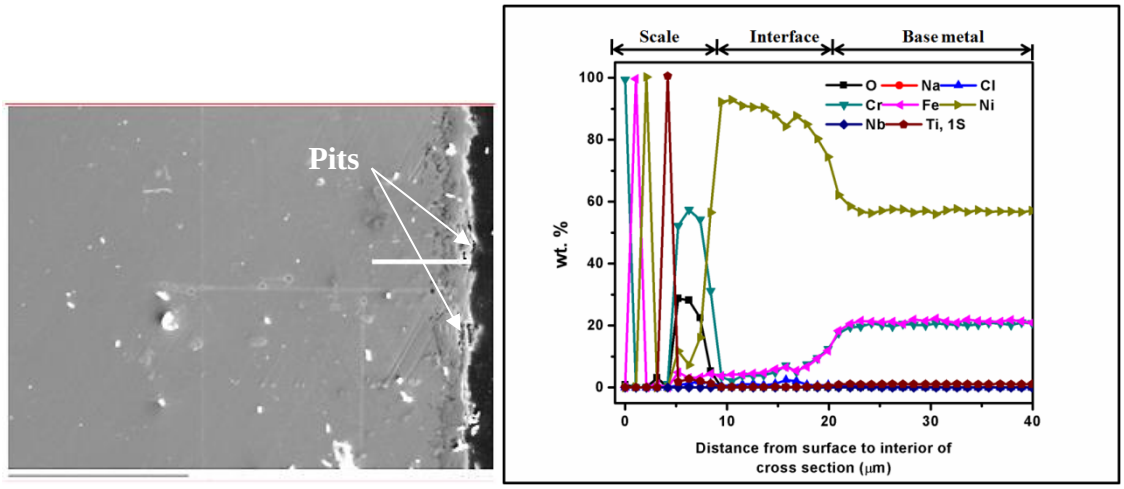

Fig. 3. 16: Elemental distribution in cross section of the specimen ground with #400, up to the depth of 40 μm from the surface, coated with 1S salt and exposed at 600ºC for 100 h.

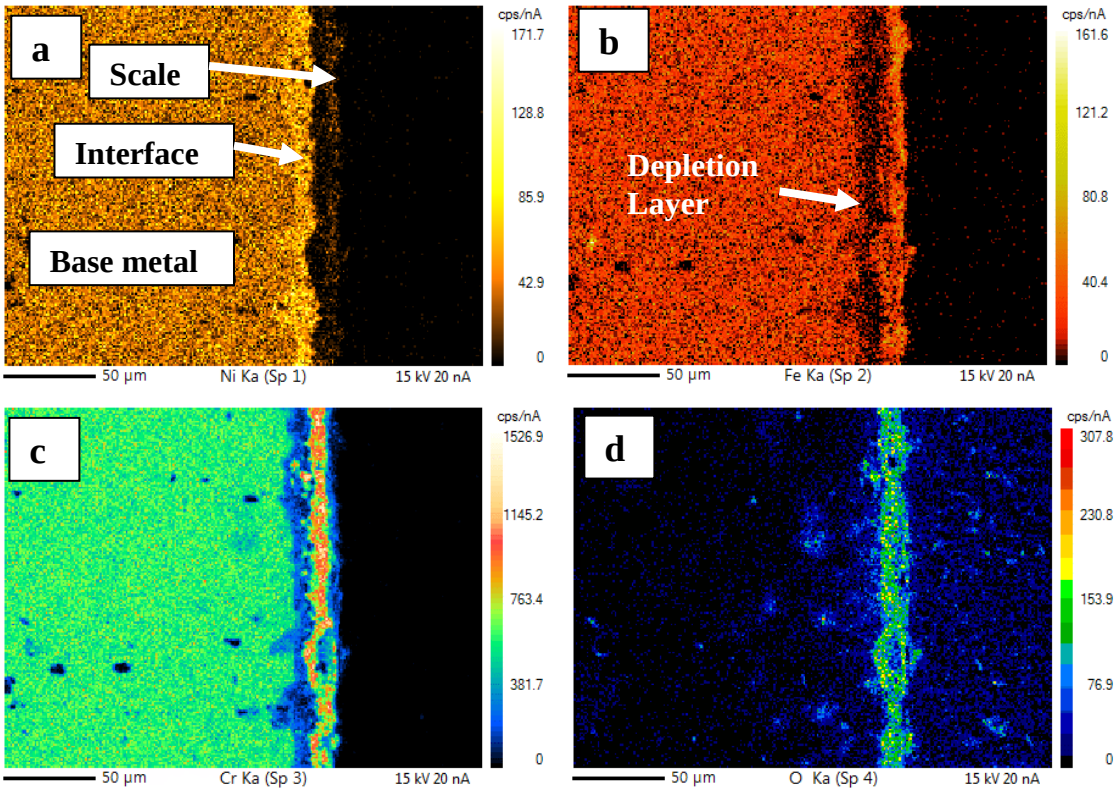

Fig. 3. 17: EPMA/SE X-ray mapping of cross section of the 1S salt coated sample exposed at 600ºC up to 100 h, showing distribution of different elements: (a) Nickel, (b) Iron, (c) Chromium and (d) Oxygen.

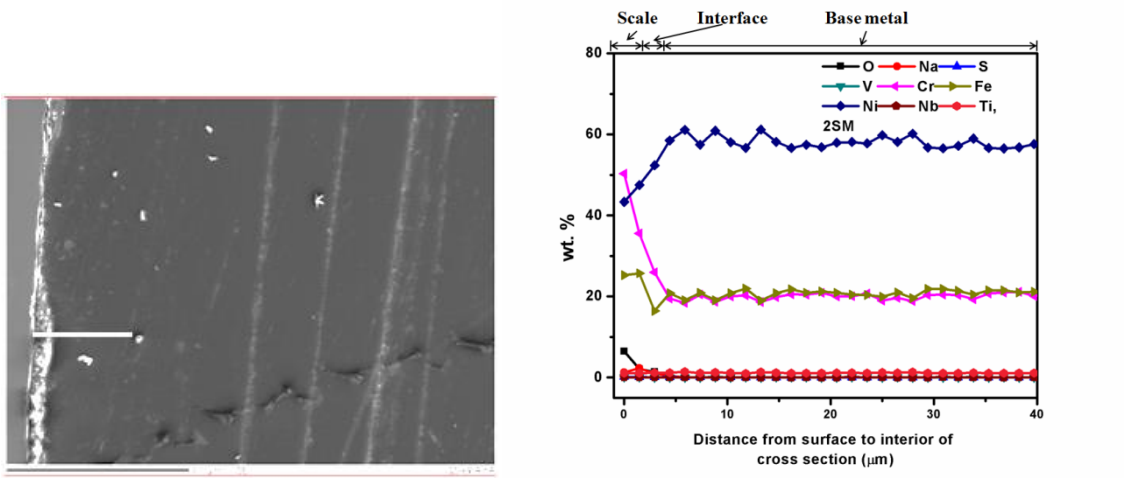

Fig. 3. 18: Elemental distribution in cross section of the specimen ground with #400, up to the depth of 40 µm from the surface, coated with 2SM salt mixture and exposed at 600ºC for 100 h.

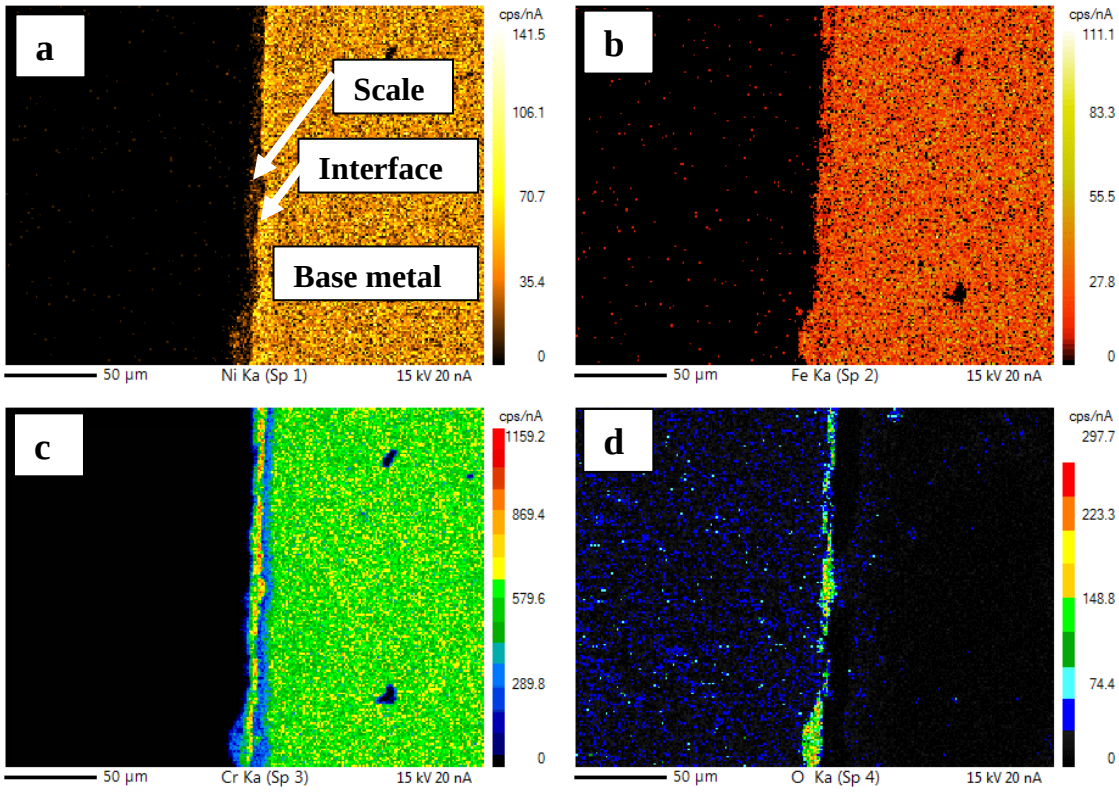

Fig. 3. 19: EPMA/SE X-ray mapping of cross section of the specimen coated with salt mixture 2SM and exposed at 600ºC for 100 h, showing distribution of different elements: (a) Nickel, (b) Iron, (c) Chromium and (d) Oxygen.

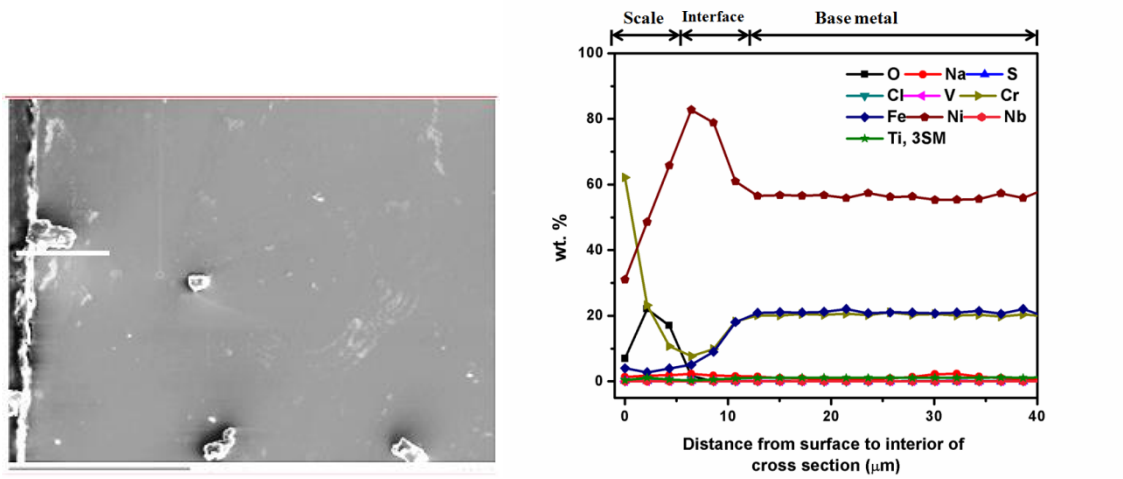

Fig. 3. 20: Elemental distribution in cross section of the specimen ground with #400, up to the depth of 40 μm from the surface, coated with 3SM salt mixture and exposed at 600ºC for 100 h.

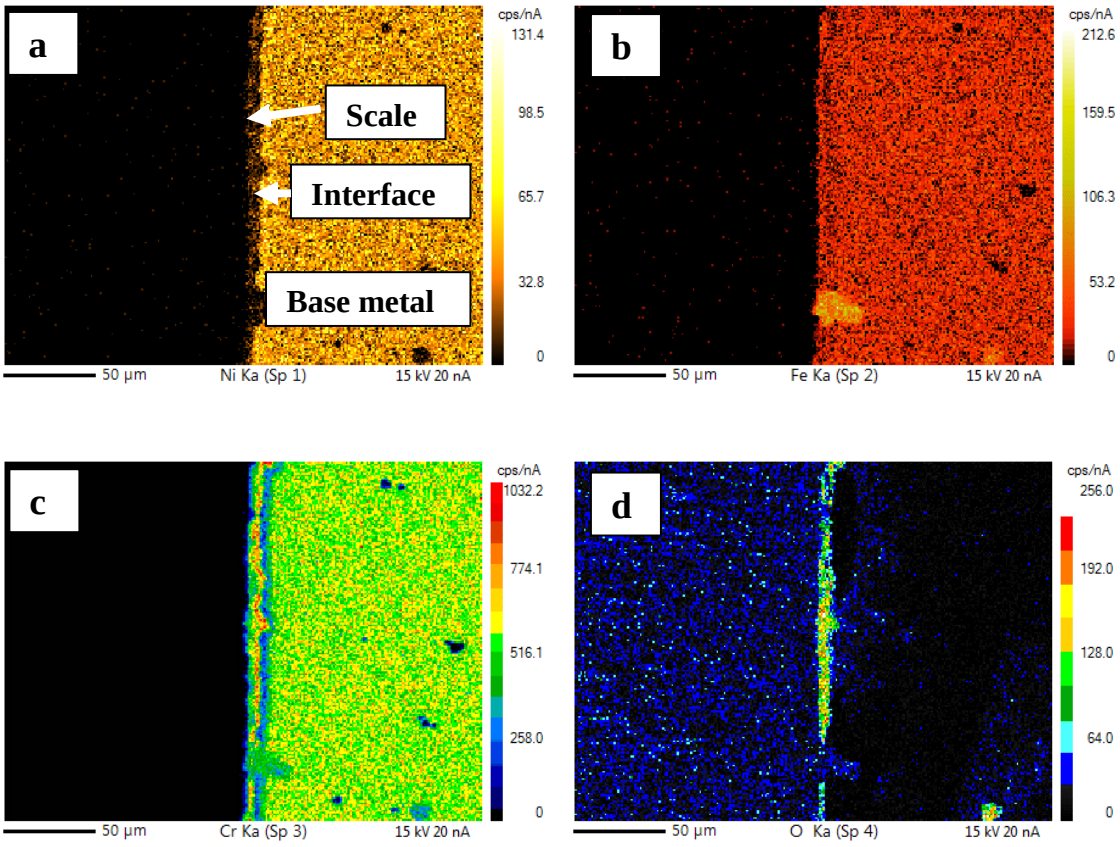

Fig. 3. 21: EPMA/SE X-ray mapping of cross section of the specimen coated with salt mixture 3SM and exposed at 600ºC for 100 h, showing distribution of different elements: (a) Nickel, (b) Iron, (c) Chromium and (d) Oxygen.

3.2.10 EFFECT OF ULTRASONIC SHOT PEENING (USP) TREATMENT

The plots of weight-gain per unit area and square of weight-gain per unit area of the non-USP treated and USP treated samples coated with 1S salt and salt mixtures 2SM and 3SM exposed at 600 °C for a period of 100 h are shown in Fig. 3.22, Fig. 3.23 and Fig. 3.24 respectively, and shows the effect of ultrasonic shot peening on the hot corrosion resistance against the exposure of salt/salt mixtures. The samples exposed to salt 1S showed highest weight-gain, followed by those exposed to 3SM and 2SM salts mixtures respectively, in both, non-USP as well as USP treated condition. The USP treated samples exposed to salt 1S and the salt mixtures of 2SM and 3SM showed linear variation in weight for the entire period of exposure. The plots of square of weight-gain/unit area (mg/cm^2) versus time (h) were used to establish the rate law for the process of hot corrosion. The rate constant (k_p) shown in Table 3.3 was calculated using the parabolic rate law equation: $(W/A)^2 = k_p t + C$, where W/A is the weight-gain per unit surface area (mg/cm^2), *t* is the time of exposure, and *C* is a constant.

Table 3.4: Parabolic rate constant (k_p) of the non USP and USP treated samples, corroded at 600^0C up to 100 h.

Material Condition	#400 polished (R_a = 0.46 µ m)		5 min USP treated (R_a = 1.43 µ m)	
	k_p	R^2	k_p	R^2
1S				
Up to 25 h	1.64	0.91	-	-
Up to 100 h	0.25	0.98	0.16	0.94
2SM				
Up to 25 h	0.10	0.97	0.01	0.92
Up to 100 h	0.10	0.97	0.01	0.92
3SM				
Up to 25 h	0.71	0.98	0.01	0.94
Up to 100 h	0.07	0.99	0.01	0.94

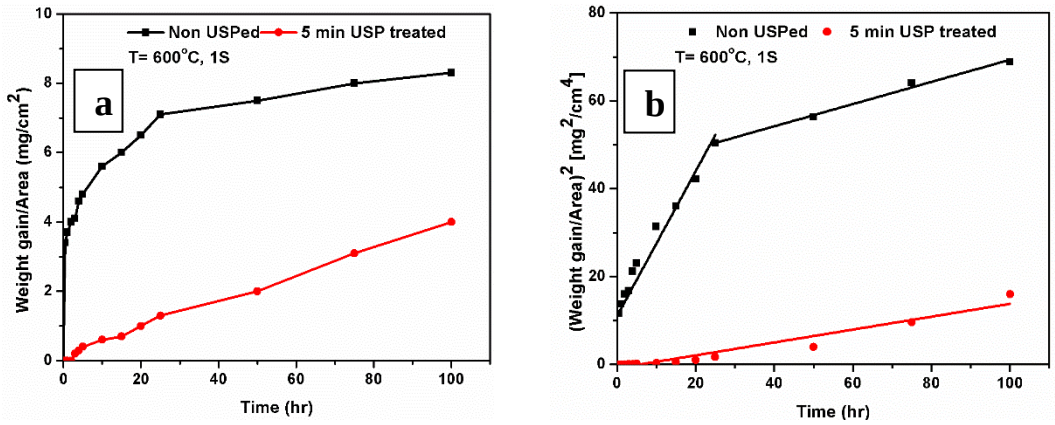

Fig. 3. 22: Effect of ultrasonic shot peening for 5 min on hot corrosion resistance of the specimens coated with 1S exposed at 600^0C, up to 100 h: (a) Weight gain per unit area vs time; (b) Square of weight gain per unit area vs time.

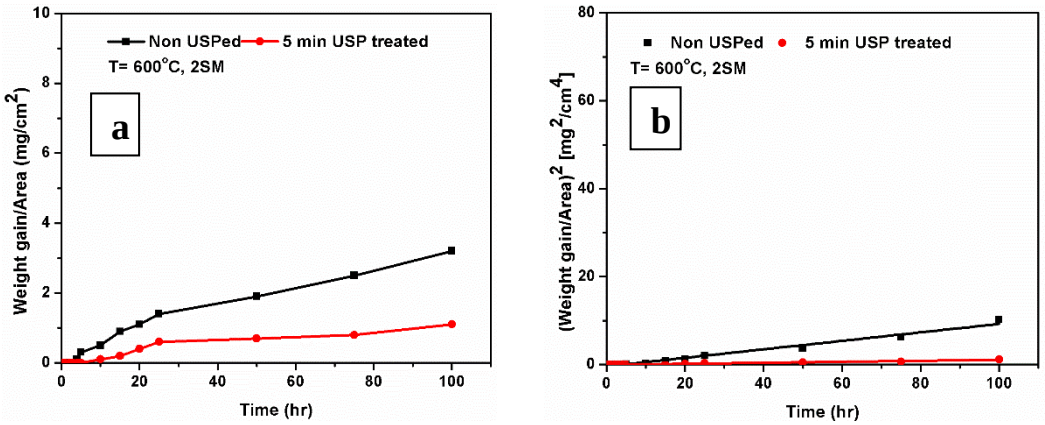

Fig. 3. 23: Effect of ultrasonic shot peening for 5 min on hot corrosion resistance of the specimens coated with 2SM exposed at 600^0C, up to 100 h: (a) Weight gain per unit area vs time; (b) Square of weight gain per unit area vs time.

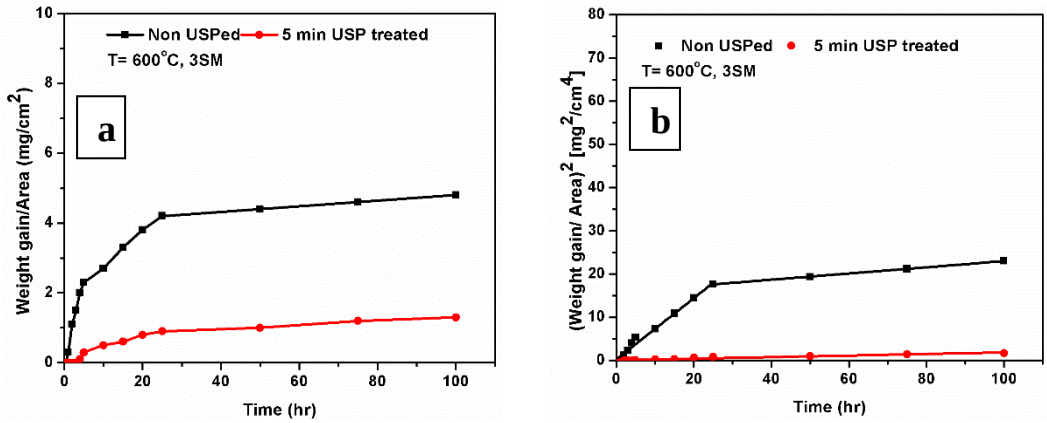

Fig. 3. 24: Effect of ultrasonic shot peening for 5 min on hot corrosion resistance of the specimens coated with 3SM exposed at 600^0C, up to 100 h: (a) Weight gain per unit area vs time; (b) Square of weight gain per unit area vs time.

The curves of weight-gain plots were best fitted by linear least-square method and the calculated values of k_p are presented in Table 3.4. It is obvious from the data in Table 3.4 that the value of k_p was higher for the sample exposed to 1S salt than for those exposed to 3SM and 2SM salt mixtures. Further, k_p was higher for the non-USP treated ones as compared to those of the USP treated condition for all the three types of salts mixture both at 600 °C.

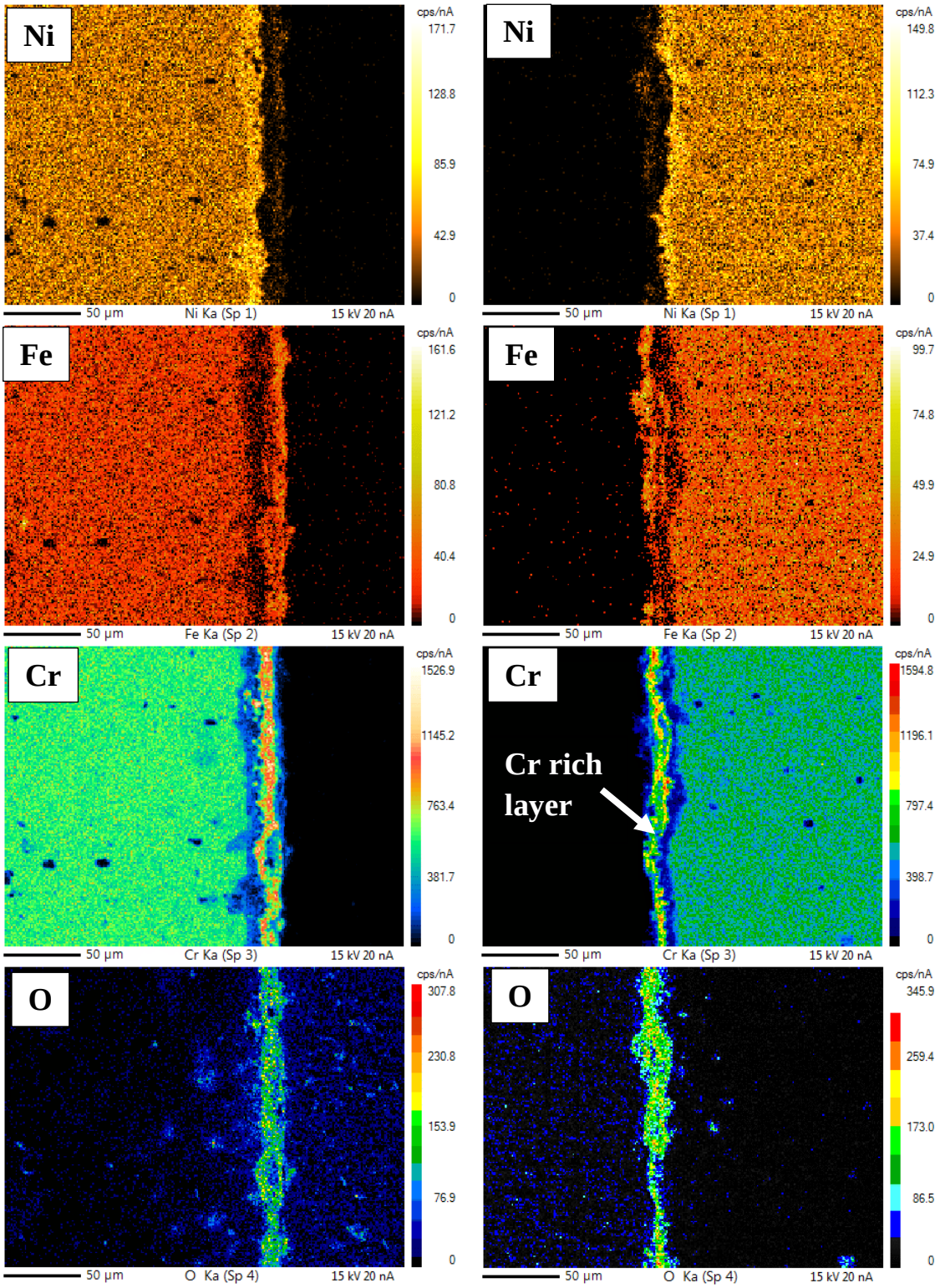

Fig. 3. 25: EPMA/SE X-ray mapping of cross sections of specimens coated with salt 1S and exposed at 600°C for 100 h, showing distribution of different elements: Nickel, Chromium, Iron and Oxygen for (a) non shot peened sample and (b) 5 min USP treated sample.

(a) Non- USP treated **(b) 5 min USP treated**

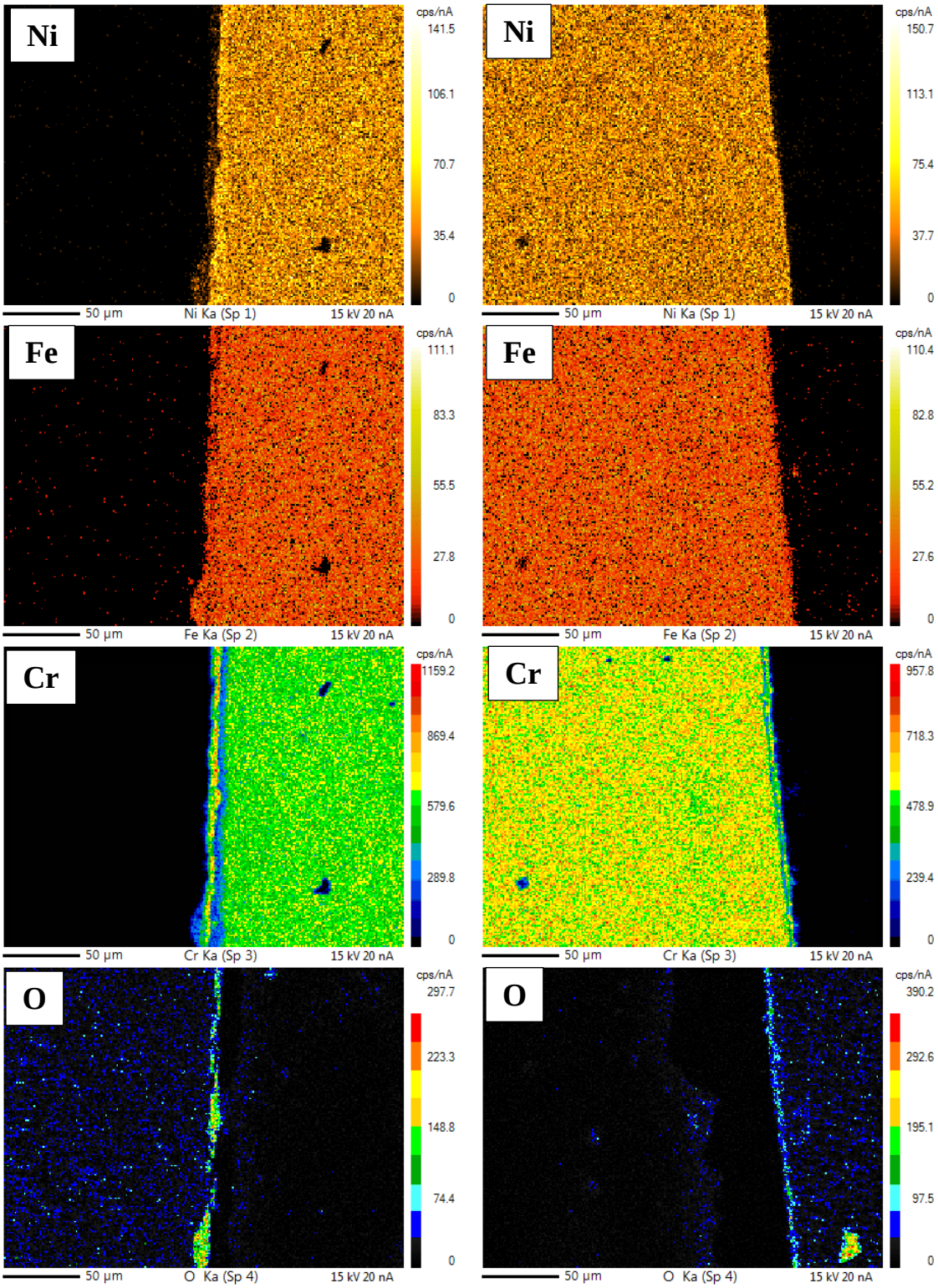

Fig. 3. 26: EPMA/SE X-ray mapping of cross sections of specimens coated with salt mixture 2SM and exposed at 600°C for 100 h, showing distribution of different elements: Nickel, Chromium, Iron and Oxygen for (a) non shot peened sample and (b) 5 min USP treated sample.

(a) Non- USP treated **(b) 5 min USP treated**

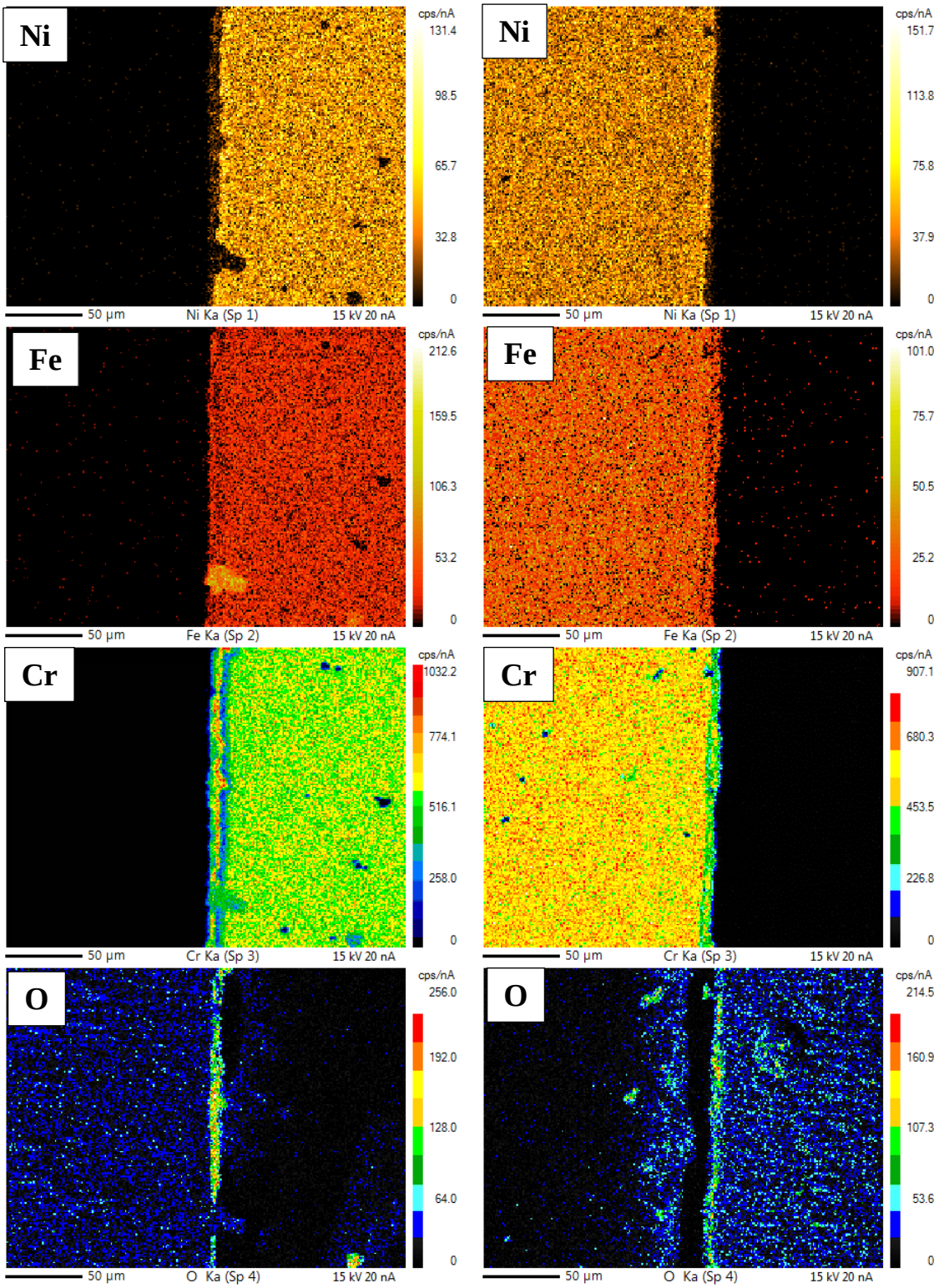

Fig. 3. 27: EPMA/SE X-ray mapping of cross sections of specimens coated with salt mixture 3SM and exposed at 600°C for 100 h, showing distribution of different elements: Nickel, Chromium, Iron and Oxygen for (a) non shot peened sample and (b) 5 min USP treated sample.

Figs. 3.25 -3.27 show EPMA of cross sections of the specimens coated with 1 S salt and 2SM and 3SM salt mixtures respectively exposed at 600°C for 100 h, showing distribution of different elements like nickel, chromium, iron and oxygen for non-shot peened and 5 min USP treated samples. It may be seen that the region of oxygen distribution is more in the non-USP treated sample than that in the USP treated one. The diffusion of chromium, iron and nickel from the base material resulted in formation of Cr_2O_3, Fe_2O_3, Fe_3O_4, NiO oxides.

3.3 DISCUSSION

The results obtained from this study clearly show that high surface roughness resulting from coarse emery paper of #400 grit, increased the rate of corrosion irrespective of the type of the salt coatings. The weight gain was highest for the sample coated with 1S salt followed by that coated with the salt mixture 3SM and was lowest for the sample coated with the salt mixture 2SM, exposed at 600ºC for 100 h. In general, it was observed from corrosion kinetics that the rough surfaces are more prone to hot corrosion as compared to the smoother ones. The weight gain vs time plots of the samples coated with salt and salt mixtures clearly followed nearly parabolic law and showed dual slope in majority of the cases. Initially the corrosion rate was slow up to 5 h but increased rapidly thereafter up to 25 h, and remained almost constant up to 100 h of exposure. It may also be noticed that NaCl was highly aggressive at 600ºC due to high volatility of chlorides. The initial 5 h may be considered as the period of incubation and the next 20 h period of aggressive attack because of continuous supply of the corrodants. The corrosion rate, however, was slowed down after 25 h in all the cases due to decrease in the available quantity of salt and salt mixtures. Surface roughness of the samples decreased with increase in grit number of the SiC coated emery papers used for

grinding of the surface. Mechanical grinding of surface causes cold deformation of the surface region and the dislocation density increases (Fig. 3.3 a). The dislocation density increases with surface roughness, likewise the microhardness also increases (Fig. 3.3 b). The deleterious effect of cold working on corrosion resistance of the austenitic stainless steels was revealed in acidic and chloride containing media **[Ozgowicz et al. (2012)]**. In the case of a rougher surface larger surface area is involved in the process of corrosion to result in high rate of corrosion **[Balsone (1985), Sidky et al. (1987)]**. The samples ground by #400 grit SiC emery paper with $R_a \approx 0.46$ µm showed highest weight gain and there was most deleterious effect in the 1S coated sample. The depth of penetration was found to be 32.9±2.3 µm, 5.2±0.7 µm and 8.1±1.1 µm from the Figs. 3.9 (a), 3.10 (a), and 3.11 (a) for the 1S, 2SM and 3SM coated samples respectively.

The samples ground by #600 grit SiC emery paper ($R_a \approx 0.28$ µm) showed higher weight gain with the 1S coating as compared with the 3SM and 2SM coatings, exposed at 600ºC up to 100 h. In this case the roughness was relatively less as compared to that ground with #400 grit, therefore the corrosive attack was relatively less. The removal of electrons was relatively more difficult for taking part in corrosion reaction, therefore the depth of penetration revealed from Figs. 3.9 (b), 3.10 (b), and 3.11 (b) was also less as 27.5±1.6 µm, 4.5±0.5 µm and 6.9±0.8 µm for the 1S, 2SM and 3SM coated samples respectively, exposed at 600ºC up to 100 h. Similarly the progressive decrease in the rate of hot corrosion of the samples coated with 1S, 2SM and 3SM in the smoother samples grinded with emery papers of finer SiC particles of #800 and #1000 grits may be understood from the Figs. 3.9 (c), 3.10 (c), 3.11 (c) and Figs. 3.9 (d), 3.10 (d), 3.11 (d). The effect of high temperature corrosion from the NaCl salt (1S) environment is discussed in detail as the rate of corrosion was highest in this case in respect of those coated with the other two salt mixtures (2SM and 3SM).

3.3.1 EFFECT OF 1S (100% NACL) COATING

A possible mechanism of corrosion due to 1S coating on the rough surface is schematically shown in Fig. 3.28. The rough surface gives more preferential sites for corrosion attack as compared to the smoother one because of greater microscopic surface area in the former. In the 1S salt environment it may be seen that the scale was cracked (Fig. 3.13).

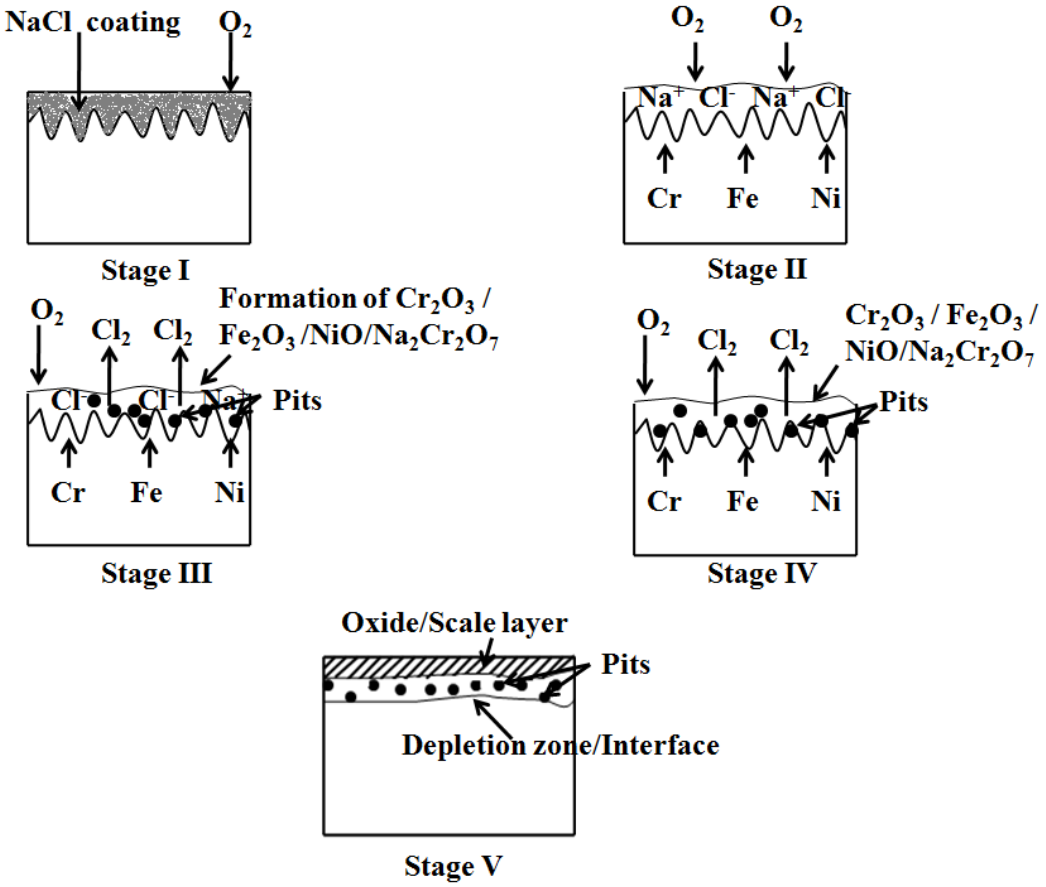

Fig. 3. 28: Schematic presentation showing the process of corrosion on the specimen with coarse surface, coated with 1S salt (100 wt% NaCl), and exposed at 600ºC up to 100 h.

The possible mechanism of NaCl induced corrosion at the surface is explained below:

Stage I: Presence of NaCl particles on the rough surface exposed at 600ºC up to 100 h (Fig. 3.28).

Stage II: Dissociation of NaCl at 600ºC into Na^+ and Cl^- ions and start of reaction between oxygen and the substrate species (Fig. 3.28).

Stage III: Rapid oxidation of chromium because of its known high negative value of ΔG and cracking of the protective oxides due to presence of NaCl. Oxychlorination reaction takes place and penetration of chlorine ion starts into the substrate through the cracked oxide scale. Thus, chlorine ions penetrate the scale interface and reach the metal/scale interface and form chlorides of Cr, Fe and Ni. Chlorine gas (Cl_2) escapes through outward diffusion from the substrate/scale interface leading to formation of pits (Fig. 3.28) as per the following reactions:

$$2CrCl_2(g) + 3/2\ O_2(g) = Cr_2O_3(s) + 2Cl_2(g) \quad (3.3)$$

$$2CrCl_3(g) + 3/2\ O_2(g) = Cr_2O_3(s) + 3Cl_2(g) \quad (3.4)$$

$$3FeCl_2(g) + 2O_2(g) = Fe_3O_4(s) + 3Cl_2(g) \quad (3.5)$$

$$2FeCl_2(g) + 3/2\ O_2(g) = Fe_2O_3(s) + 2Cl_2(g) \quad (3.6)$$

$$NiCl_2(g) + 1/2\ O_2(g) = NiO(s) + Cl_2(g) \quad (3.7)$$

Sodium ions combine with oxygen and form Na_2O which reacts with chromium oxide and oxygen through inward diffusion to form $Na_2Cr_2O_7$.

Stage IV: Stages III and IV (Fig. 3.28) continue till all the NaCl gets consumed.

Stage V: Formation of oxide scale and depletion zone of alloying elements takes place due to continuous and simultaneous reactions as shown in Fig. 3.28. Thus, the rough surface produces large depth of penetration as compared to the smoother ones (Fig. 3.9).

The salt induced corrosion in 100 wt% NaCl was in agreement with earlier investigation of **Mahobia et al. (2013)** at 550 and 650ºC.

For the smoother surfaces also the mechanism of corrosion remains the same as the above, the only difference being in the depth of penetration of the corrodants. The smoother surface showed higher corrosion resistance and smaller zone of depletion of alloying elements (Fig. 3.9d).

The mechanism suggested above was supported from the results obtained by XRD/SEM/EDS studies of the corrosion products formed on the surface of the superalloy (Fig. 3.12 b, Fig. 3.13.). Chlorine is released as per the above reactions from 3.2 to 3.7 and reacts with the oxides and alloying elements to form their volatile chlorides. The EPMA results were also in agreement with the above reactions and showed that concentration of Fe was maximum followed by those of Cr, Ni, and oxygen in the corroded region and there were distinct adjacent zones of depletion of these elements. The concentration of Cr and Nb in the surface region is relatively less as compared with that of Fe which may be attributed to their lower diffusivity. It shows that the activity of Fe in the corrosion reactions is more as it is depleted more from the substrate (Fig. 3.17). Here, it is noteworthy that elemental mapping (Fig. 3.16) from the surface to interior supports the EPMA results.

3.3.2 FFECT OF 2SM (60% NA_2SO_4 + 40% V_2O_5) SALT COATING

The sample exposed to salt mixture of 2SM showed much less weight gain (Figs. 3.7 (a) and (b)) as compared with those exposed in the 1S salt and the 3SM salt mixture at 600ºC up to 100 h (Figs. 3.6 (a), (b) and 3.8 (a), (b)), mainly due to absence of NaCl salt. The surface morphology and composition analysis are shown in Fig. 3.14.

Some possible oxidation reactions with this salt mixture are presented below in the equations (3.8- 3.13):

$2Cr + 3/2\ O_2 = Cr_2O_3$ (3.8)

$2Fe + 3/2\ O_2 = Fe_2O_3$ (3.9)

$Ni + 1/2\ O_2 = NiO$ (3.10)

$NiO + Cr_2O_3 = NiCr_2O_4$ (3.11)

$FeO + Cr_2O_3 = FeCr_2O_4$ (3.12)

$NiO + Fe_2O_3 = NiFe_2O_4$ (3.13)

Also, formation of $Na_2Cr_2O_7$ occurs as per the following reaction:

$Na_2O + Cr_2O_3 + 3/2\ O_2 = Na_2Cr_2O_7$ (3.14)

Here also surface roughness plays important role. The sample with roughest surface showed highest weight gain whereas the smoother ones showed negligible weight gain. From cross sectional elemental mapping of the hot corroded, sample almost no change in the composition, except the slight change in oxygen, vanadium and sulphur was observed at the surface (Fig. 3.18). EPMA results also support the above statement as shown in Fig. 3.19.

3.3.3 EFFECT OF 3SM (75%NA_2SO_4+ 15 % NACL + 10% V_2O_5) COATING

Fig. 3.11 shows cross sectional view of hot corroded samples of the 3SM coated sample, exposed at 600ºC up to 100 h. Oxide layer and region of depletion with pits were observed in the corroded sample. Basic fluxing mechanism leads to formation of Cr_2O_3 and non-protective NiO oxide **[Kamal et al. (2010), Stringer (1973)]**. Cr content was less in the depleted region as compared with that in the oxide layer and the other alloying elements. Due to NaCl attack pits were observed at the grain boundaries as well as in the interior of the grains. EPMA analysis (Fig. 3.21) clearly revealed diffusion of alloying

elements from the substrate to surface and that of the corrodants from the surface into the substrate. Elemental mapping (Fig. 3.20) was also in line with the EPMA results.

Formation of oxides was confirmed by XRD analysis of the sample coated with 3SM salt mixture (Fig. 3.12 (d)). It is important to understand the mechanism of hot corrosion from the initial to the final stage. Due to presence of chlorine in the form of NaCl in the 3SM salt mixture, metallic chlorides are formed and evaporate continuously **[Albina (2005)]**. Gaseous chlorides react with oxygen in the scale to form solid oxides and release gaseous chlorine **[Albina (2005), Zahs (2000)]**. NaCl reacts with Cr_2O_3 and forms Na_2CrO_4 with yellow appearance throughout the sample in the form of spots **[Mannava et al. (2016), Gurrappa (1999)]**. Pits were formed in the cross section wherever metal chlorides evaporated (Fig. 3.11 (a)). V_2O_5 reacted with Cr_2O_3, Fe_2O_3 and NiO and formed vanadate compounds. Sulphur ions react with Cr, Fe and Ni or their oxides and form respective sulphides **[Mannava et al. (2016)]**. In the 3SM coated samples first a thin layer of oxides of the elements like Cr, Fe, Ti, and Nb formed during the first few h, followed by formation of traces of some chlorides/sulfides [$FeCl_3$, $TiCl_3$, and NiS, FeS, NbS_2] which slowly enhanced the process of corrosion in the later stages. Corrosion rate was slow due to low contents of NaCl (15 wt.%) and V_2O_5 (10 wt.%) in the 3SM. The scale formed was adherent, impervious and there was no spalling of the scale. Formation of the scale rich in $NiCr_2O_4$ contributed for the better corrosion resistance **[Gurrappa (1999)]**. Thus, corrosion of the superalloy IN718 with 3SM salt coating, at 600ºC, was primarily by the process of oxidation, followed by slow oxychlorination/sulfidation reactions.

Furthermore, corrosion resistance is found to be enhanced by the novel process of ultrasonic shot peening. The presence of Cr_2O_3 layer on the shot peened samples

resulted in improved corrosion resistance of the alloy because of extensive grain refinement at the surface. These results are in agreement with the earlier investigation **[Matsuo (2004)]**. Here, the diffusivity of chromium increases with increase in the population of grain boundaries which leads to formation of highly protective Cr_2O_3 as compared to that in the non-shot peened one **[Tan et al. (2008)].** Oxygen diffusivity is increased on the modified surface before the formation of protective layer and it is decreased after the formation of protective layer by covering the grain boundaries on the shot peened surface **[Kumar et al. (2016), Wang et al. (2003)]**. The more protective effect of the oxide layer of Cr_2O_3 formed at 700ºC on the USP treated surface is quite evident from the much better uniformity and higher thickness of the compact Cr_2O_3 layer formed on the USP treated sample (Figs. 3.25-3.27).

3.4 CONCLUSIONS

Corrosion behavior of the superalloy IN718 was studied with different surface roughness, in simulated marine environments, at 600ºC for a period up to 100 h. The following conclusions are drawn:

a) Corrosion was found to increase with the roughness of the surface due to increase in the surface area for the corrosive attack.
b) Heavy scaling and spalling of scale occurred in the 1S coated sample, however, the scale formed on the 2SM coated sample was more adherent and there was very less scaling in the 3SM coated sample, with yellow spots of Na_2CrO_4.
c) Corrosion rate was found to be highest for the 1S coated sample followed by those coated with 3SM and 2SM respectively.

d) Chlorides in the form of volatile species led to formation of voids and pits and thus provided easy path for the flow of corrodants in the 1S coated specimens. On the other hand the salt mixture of 3SM exhibited slight corrosive action due to much lower content of NaCl. The corrosion was least in the specimen coated with the salt mixture of 2SM due to absence of NaCl in it.

e) In general, corrosion kinetics was lower in the specimens subjected to USP treatment having Cr rich oxide and surface nanostructure.